

## SEBASS imaging for Copper Porphyry and Skarn Deposits, Yerington, NV

Riley, D. <sup>[1]</sup>, Cudahy, T. <sup>[2]</sup>, Hewson, R. <sup>[2]</sup>, Jansing, D. <sup>[1]</sup>, Hackwell, J. <sup>[3]</sup>

- 
1. The Aerospace Corporation, Chantilly, VA, USA
  2. CSIRO Exploration and Mining, Kensington, WA, Australia
  3. The Aerospace Corporation, El Segundo, CA, USA

### ABSTRACT

*Copper porphyry and skarn deposits have numerous alteration and rock forming minerals with absorption features in the long wave infrared (LWIR). Airborne visible-near infrared (VNIR) – short wave infrared (SWIR) imaging spectrometers can remotely map many of the minerals associated with propylitic, argillic, phyllic, and potassic alteration. Quartz, feldspars, garnets and pyroxenes are common minerals associated with these deposits and VNIR-SWIR hyperspectral sensors are not well suited for their identification. SEBASS (Spatially Enhanced Broadband Array Spectrograph System) is a hyperspectral sensor that measures from 2.5 – 5.3  $\mu\text{m}$  and 7.5-13.5  $\mu\text{m}$  from an aircraft or the ground. This mineral mapping of quartz, feldspars, garnets, pyroxenes, and olivine in the LWIR provides new and complimentary data that is useful for mineral exploration. Carbonates, sulfates, and hydroxide minerals (micas and clays) can be mapped remotely in the LWIR in addition to SWIR. This use of the LWIR for mapping carbonates, sulfates, and hydroxides provides additional information since many of these minerals have absorption features that overlap in the SWIR. SEBASS was flown over several copper porphyry and skarn deposits in the Yerington, NV mining district in September, 1999. At-sensor data were corrected for atmospheric effects using In Scene Atmospheric Correction (ISAC) and the resulting apparent surface radiance data were then corrected to apparent emissivity using an emissivity normalization algorithm. Mineral maps were created using publicly available spectral signature libraries using a spectral feature analysis algorithm. Alteration assemblage maps were also created from these remotely mapped minerals. A good correlation exists between the spatial distribution of these minerals maps and previous work that used a matched filter algorithm with ground truth data. This study shows that LWIR hyperspectral data are useful for remotely mapping of alteration and rock forming minerals commonly associated copper porphyry and skarn deposits.*

### INTRODUCTION

Spectral absorption features of alteration minerals associated with porphyry copper and skarn deposits are present in the long wave infrared (LWIR, 8.0-14.0  $\mu\text{m}$ ) as well as the visible near infrared (VNIR, 0.4-1.1  $\mu\text{m}$ ) and through the short wave infrared (SWIR, 1.1-2.5  $\mu\text{m}$ ) (Abrams et al., 1983; Spatz and Wilson, 1995). Airborne hyperspectral sensors can remotely map these minerals using their associated spectral absorption features. Since porphyry copper and skarn deposits commonly produce zoned assemblages of these alteration minerals (Lowell and Guilbert, 1970) this indicates that these zonal assemblages can be mapped remotely.

SEBASS (Spatially Enhanced Broadband Array Spectrograph System) measures the reflected and emitted radiation in the 2.5 – 5.3  $\mu\text{m}$  wavelength region with 128 bands and the emitted radiation with 128 bands in the 7.5 – 13.5  $\mu\text{m}$  wavelength region with a 1.1 milliradian field of view (1mrad FOV) per pixel. This sensor is commonly flown at 2000m above

ground level (AGL) producing a 2m resolution, but can be flown at lower or higher altitudes. The signal to noise resolution has been tested at over 2000:1 with greater area coverage (Hackwell et al., 1996).

This study was conducted 1) to determine if a spectral feature analysis algorithm could remotely map the hydrothermal alteration associated with a porphyry copper district; 2) can hydrothermal alteration be remotely mapped using a simple deposit model and publicly available mineral spectral libraries with no ground truth measurements. The altered rocks of the porphyry and skarn deposits in Yerington, Nevada are well exposed and have been mapped in extensive detail. Moreover, the rocks have been tilted almost 90° exposing propylitic, argillic, phyllic, and potassic alteration with the porphyry copper deposit and the hydrothermal fluid paths have been mapped to the associated skarn deposits (Dilles and Proffett, 2000). Earlier multispectral and hyperspectral sensing studies (Windeler and Lyon, 1991; Cudahy et al., 2000) combined with the detailed mapping of the hydrothermal alteration and lithology (Dilles and

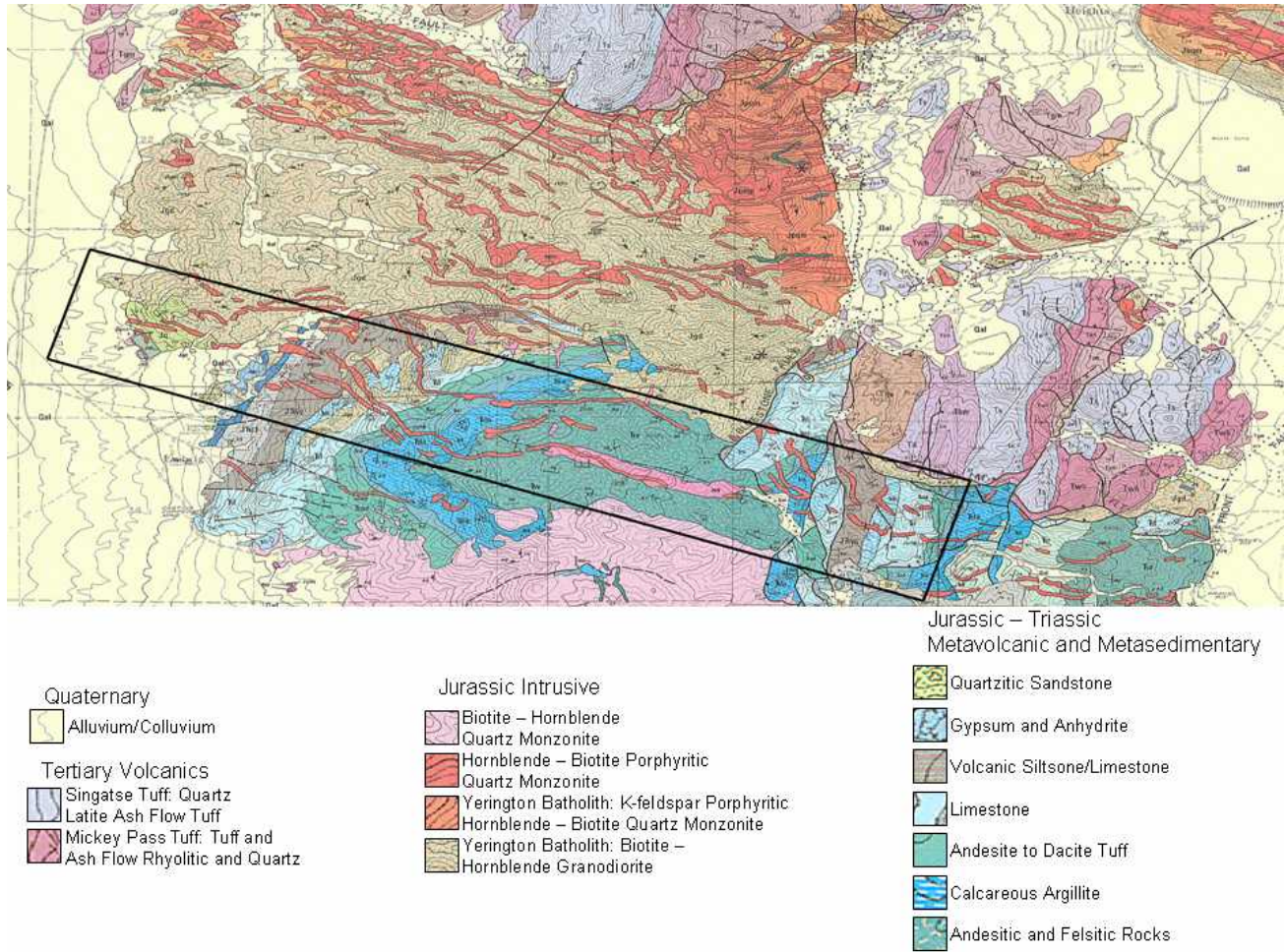


**Figure 1:** Modified 1:24,000 scale geology map from Proffett and Dilles (1984). Ludwig flight line outlined in black was processed using spectral feature fitting.

Einaudi, 1992; Proffett and Dilles, 1984, Figure 1) provide alternate methods for validating the proposed method using the spectral feature analysis algorithm with publicly available mineral spectral libraries

Alteration minerals associated with porphyry copper and skarn deposits and their long wave infrared absorption features are described in this paper. Deposit mapping of the hydrothermal alteration using a spectral feature algorithm are described as well. Moreover, this methodology shows the utility of mineral mapping using the long wave infrared for providing information about targets during regional and prospect exploration.

## METHODS

SEBASS data were collected in 1999 over the Yerington district and converted to calibrated radiance data. This data was atmospherically corrected using an In Scene Atmospheric Correction (ISAC) algorithm (Young et al., 2002) and converted to apparent emissivity using a temperature emissivity normalization algorithm. The LWIR data was reduced from 128

bands to 85 bands corresponding to the 8.0 – 12.0  $\mu\text{m}$  prior to spectral feature analysis. Mineral signatures from the Johns Hopkins University Spectral Library (Salisbury et al., 1991), Arizona State University Thermal Emission Spectral Library (Christensen et al., 2000), and NASA’s Jet Propulsion Laboratory ASTER Spectral Library were chosen based on the minerals in our deposit model for porphyry copper and skarns. These mineral signatures were then processed using a spectral feature fitting algorithm. A gray scale image resulted and a threshold of 2 was chosen as accurate mapping of the selected signature. Some of the other minerals that are unique in the area were remotely mapped as well.

## DISCUSSION

Propylitic minerals such as chlorite, epidote, calcite, and albite all have different absorption features in the LWIR (Figure 2). Chlorite has a deep absorption feature at 9.75  $\mu\text{m}$  and two shallower absorption features at 9.35 and 10.4  $\mu\text{m}$ . Absorption features for epidote are at 8.9, 9.4, 10.4, and 11.25  $\mu\text{m}$ . Calcite

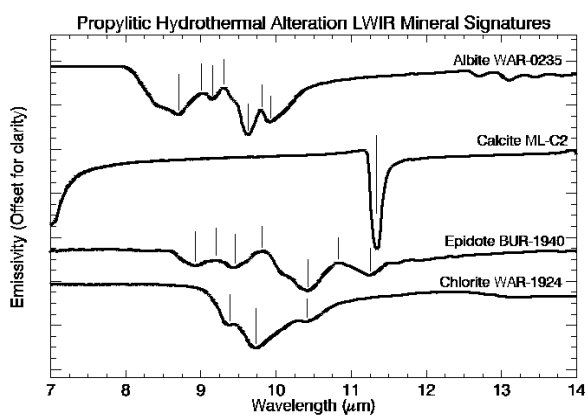


**Figure 2:** Laboratory emissivity spectra of minerals associated with propylitic hydrothermal alteration. Spectra are from the ASU TES Library (Christensen et al., 2000).

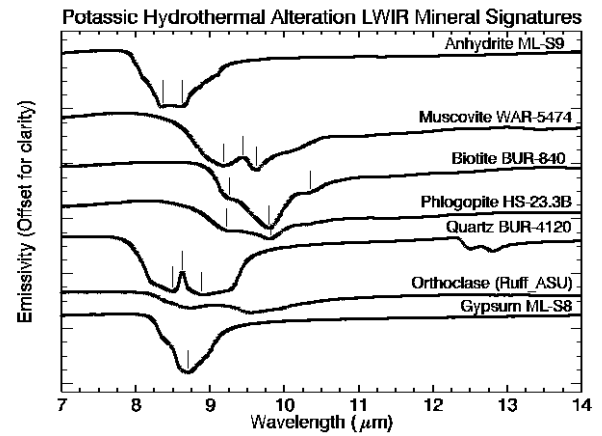


**Figure 5:** Laboratory emissivity spectra of minerals associated with potassic hydrothermal alteration. Spectra are from the ASU TES Library (Christensen et al., 2000).

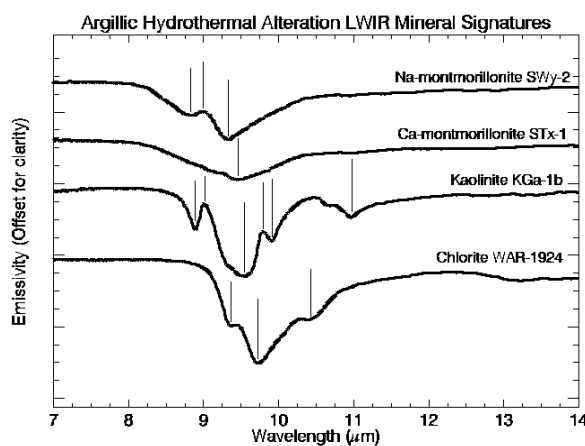


**Figure 3:** Laboratory emissivity spectra of minerals associated with argillic hydrothermal alteration. Spectra are from the ASU TES Library (Christensen et al., 2000).

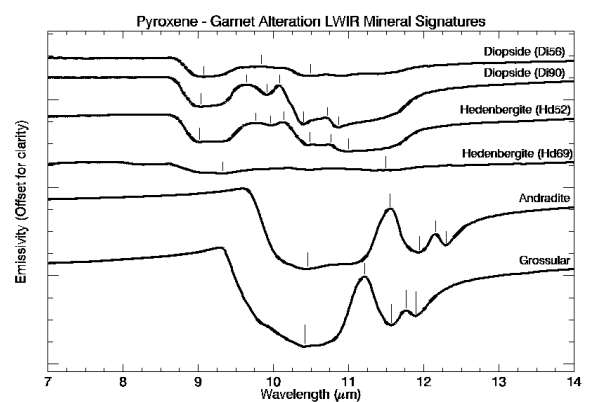


**Figure 6:** Laboratory emissivity spectra of garnets and pyroxenes associated with skarn alteration. Pyroxene spectra are from the ASU TES Library (Christensen et al., 2000) and the garnet spectra are from the JHU Spectral Library (Salisbury et al., 1991).

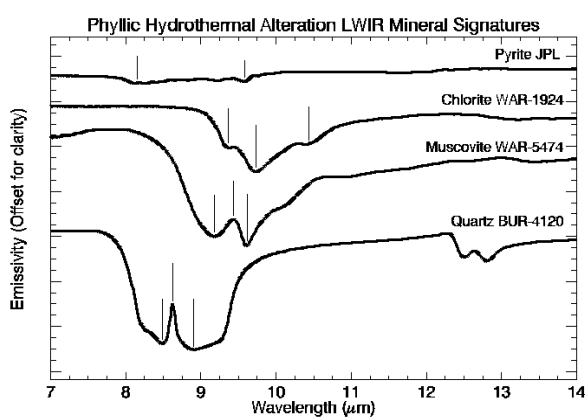


**Figure 4:** Laboratory emissivity spectra of minerals associated with phyllic hydrothermal alteration. Spectra are from the ASU TES Library (Christensen et al., 2000) and ASTER Spectral Library (<http://speclib.jp.nasa.gov>).

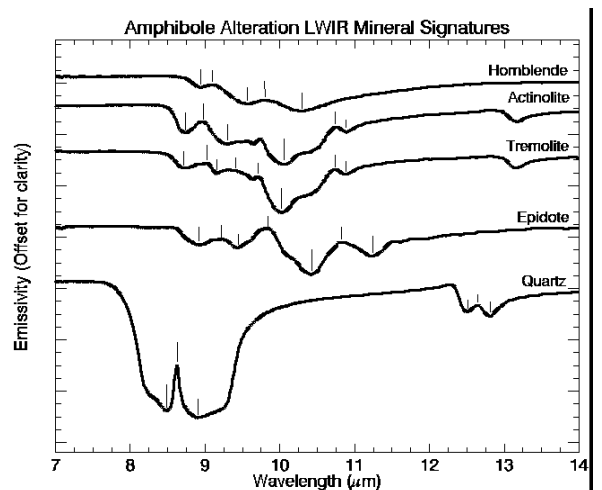


**Figure 7:** Laboratory emissivity spectra of amphiboles associated with skarn and sodic-calcic alteration. Spectra are from the ASU TES Library (Christensen et al., 2000).

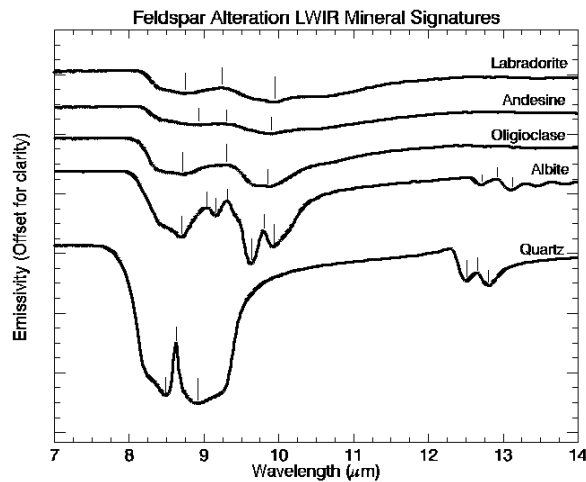


**Figure 8:** Laboratory emissivity spectra of feldspars associated with sodic-calcic alteration and country rock lithology. Spectra are from the ASU TES Library (Christensen et al., 2000).

has a single absorption feature at 11.3 μm. 8.7, 9.2, 9.6, and 9.9 μm are the absorption features of albite.

Chlorite, montmorillonite, and kaolinite are argillic hydrothermal alteration minerals and have different LWIR signatures (Figure 3). Na-montmorillonite has its primary absorption feature at 9.4 μm with a secondary feature at 8.8 μm. A broad absorption feature at 9.5 μm is representative of Ca-montmorillonite. Kaolinite has four absorption features (8.9 μm, 9.6 μm, 9.9 μm, and 11.0 μm) with the 9.6 μm and 11.0 μm features being the most significant. Chlorite’s absorption features are described in the preceding paragraph.

Phyllic alteration is usually made up of quartz, muscovite (sericite), and pyrite and their LWIR signatures are shown in Figure 4. Quartz has a unique doublet centered at 8.6 μm with the minima at 8.5 and 8.9 μm with a second doublet at 12.6 μm and minima at 12.5 and 12.8 μm. Muscovite has two absorption features at 9.25 and 9.4 μm. Pyrite’s spectra is relatively flat from 7- 14 μm with two minor absorption features at 8.2 and 9.6 μm.

Minerals typically associated with potassic alteration are orthoclase, biotite, quartz, muscovite, and anhydrite. These minerals all have LWIR signatures and phlogopite is included as the Mg-endmember of biotite (Figure 5). Quartz and muscovite signatures were discussed above. Anhydrite has a broad absorption feature at 8.5 μm and gypsums absorption feature is at 8.7 μm. Orthoclase has two absorption features at 8.75 μm and 9.5 μm. Biotite and phlogopite have similar absorption features with the minima centered at 9.8 μm. There are some subtle differences between these minerals as biotite appears to have a shallow absorption feature at 10.3 μm and phlogopite appears to have a broader absorption than biotite (Figure 5).

Diopside, hedenbergite, andradite, and grossular are common skarn minerals and their LWIR mineral signatures are shown in Figure 5. Grossular and andradite have maxima at 11.22 μm and 11.75 μm, and 11.57 μm and 12.14 μm, respectively. Their minima are at 10.39 μm, 11.57 μm, and 11.89 μm for grossular, whereas, andradite minima are at 10.43 μm, 11.92 μm, and 12.31 μm. Diopside and hedenbergite have

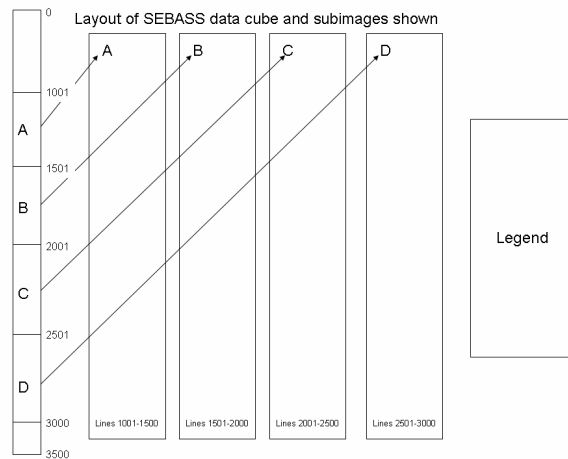


**Figure 9:** This is a reference layout of the SEBASS data cube that was processed and the images of the full flight line, and images of specific line numbers with a mineralogical legend. 1 is the entire image, 3500 lines. A is an image from lines 1000 to 1500, B is an image from lines 1501 to 2000, C is an image from lines 2001 to 2500, and D is an image from lines 2501 to 3000.

different signatures, but their maxima are near 9.8 μm and their minima are near 9.1 μm.

Amphiboles and epidote have different LWIR signatures with multiple absorption features (Figure 7). These minerals along with the feldspar minerals (Figure 8) are common skarn and sodic-calcic alteration minerals in the Yerington district (Dilles, 2000). Hornblende has its primary absorption feature at 10.25 μm and is much broader than actinolite, tremolite, or epidote. The primary absorption features of actinolite and tremolite are at 10.1 μm and 10.0 μm, respectively. Absorption features in epidote were discussed in the propylitic alteration. Albite, oligoclase, andesine and labradorite have multiple LWIR absorption features (Figure 8). Absorption features for albite are described in the paragraph regarding propylitic alteration. Oligoclase, andesine, and labradorite have two absorption features, one near 8.75 μm and the other near

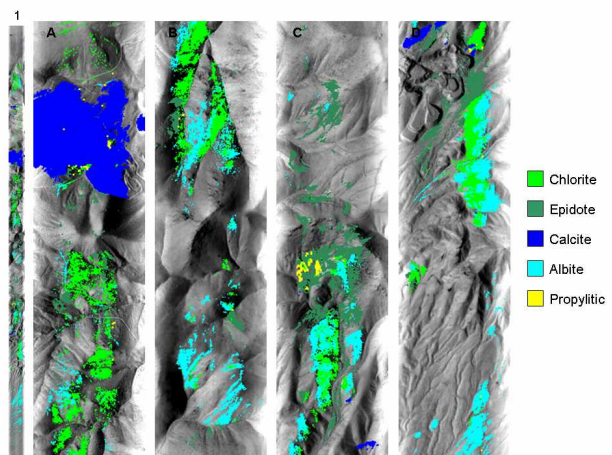


**Figure 10:** Spectral feature processing results of propylitic alteration minerals overlain on a temperature image.

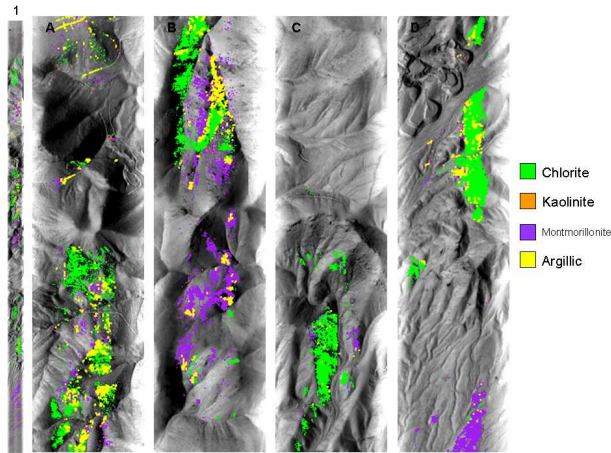


Figure 11: Spectral feature processing results of argillic alteration minerals overlain on a temperature image.

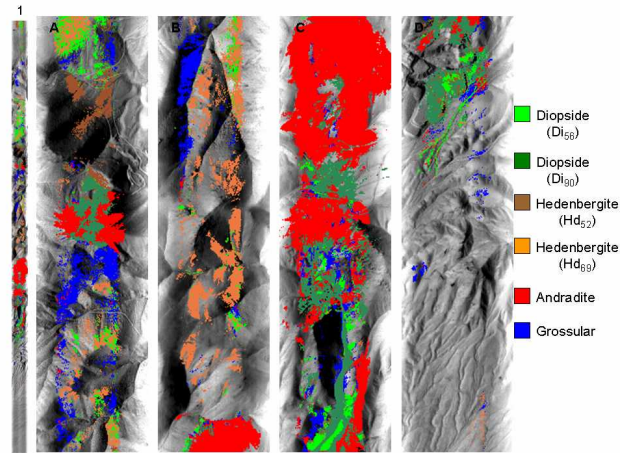


Figure 14: Spectral feature processing results of skarn alteration minerals overlain on a temperature image.

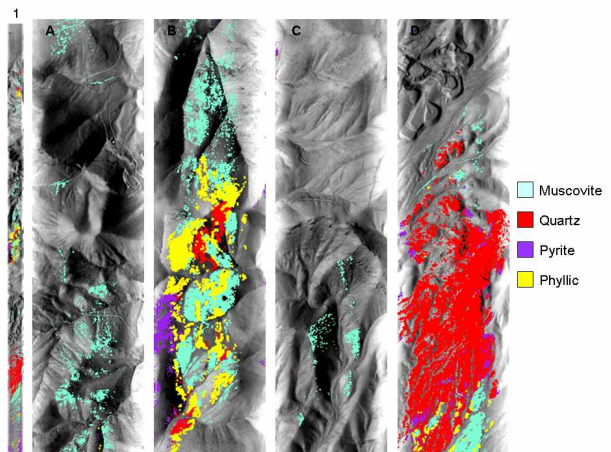


Figure 12: Spectral feature processing results of phyllic alteration minerals overlain on a temperature image.

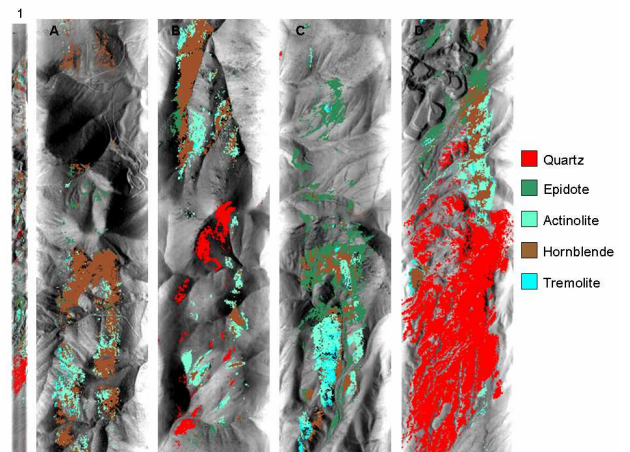


Figure 15: Spectral feature processing results of hornfels and sodic-calcic alteration minerals overlain on a temperature image.

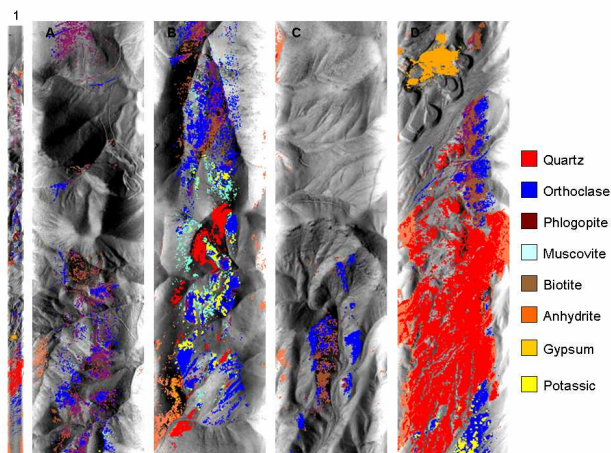


Figure 13: Spectral feature processing results of potassic alteration minerals overlain on a temperature image.

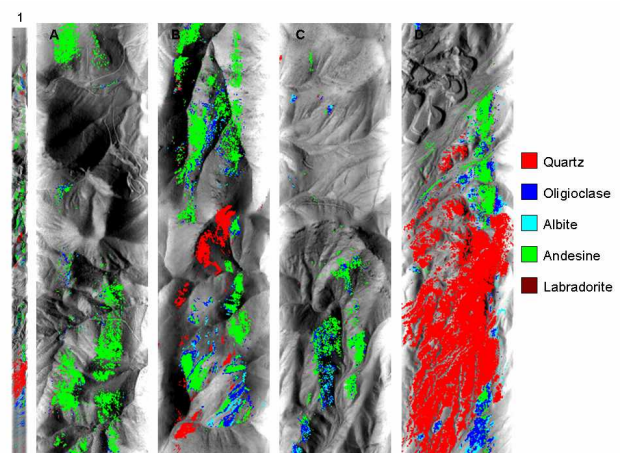


Figure 16: Spectral feature processing results of feldspars associated with skarn, hornfels, and sodic-calcic alteration overlain on a temperature image.

9.9  $\mu\text{m}$ . The absorption features of quartz were discussed in the paragraph describing phyllic alteration.

Spectral feature analysis was applied to SEBASS apparent emissivity data using publicly available library spectra (Figures 2-8). Matching image spectra with library spectra or in-scene reference spectra using the absorption features of the spectra is spectral feature fitting (Clark et al., 1990). Figure 9 is reference figure on the layout of the results that are presented in figures 10-16. Results from spectral feature fitting algorithm using the library spectra the minerals are shown in Figures 10-16.

Coherent patterns for each spectrum were produced (Figures 10-16) using the SEBASS data converted to apparent emissivity using the library spectra (Figures 2-8) and a spectral feature fitting algorithm. Propylitic, argillic, and phyllic classes are the combined spectral responses of minerals that were mapped separately. These results show a general distribution of these minerals through out the scene. However, there are some near linear classification within the scene such as chlorite in Figure 10. These near linear classifications could be the result of sensor artifacts or the low threshold used for classification. If these near linear features are the result of sensor artifacts, this aliasing artifact was introduced into the data because of under sampling in the spectral direction. Spectral interpolation near strong atmospheric features gives rise to an artifact in the data along the scan direction. This problem was fixed several years ago; current SEBASS data does not have this problem. If these near linear classifications were the result of a low threshold, a higher threshold could be used but this may eliminate pixels that have significant amounts of the mineral. Overall, the classification images show coherent patterns and suggest that spectral feature fitting is a potentially effective method of mineral mapping with SEBASS data.

Comparison of the spectral classes shows that there is some potential misidentification. Quartz, epidote, and diopside (Di90) show the potential for this misidentification (Figures 10, 12, and 14, respectively). Figure 15 shows that this misidentification between epidote and quartz can be resolved when the mineral spectra are processed together. Also, diopside and andradite are commonly found together in this district (Dilles et al., 2000) and the current spectral feature fitting algorithm maps only one spectral feature and does not provide estimates of mixing. Albite, oligoclase, andesine, and labradorite were mapped and they have some association with the pyroxenes (Figures 14 and 16).

## CONCLUSION

Spectral feature analysis of the SEBASS data allowed the discrimination of minerals associated with propylitic, argillic, phyllic, and potassic hydrothermal alteration. Minerals that are associated with skarn alteration such as garnets, pyroxenes, amphiboles, and feldspars were also mapped remotely using spectral feature analysis. These results show that hyperspectral airborne emissivity data collected from 7.5-13.5  $\mu\text{m}$  wavelength region can map minerals associated with porphyry copper and skarn deposits. Some of the minerals mapped were primary minerals (i.e. andradite and diopside) and other minerals were secondary or smaller components of the image spectra (i.e.

kaolinite). This analysis of minerals associated with propylitic, argillic, phyllic, or potassic alteration along with minerals that are associated with skarn deposits provided information about the distribution of these minerals which characterizes the porphyry copper hydrothermal alteration.

## ACKNOWLEDGEMENTS

We would like to thank Steve Ruff at Arizona State University for providing some additional LWIR spectra of feldspars from his dissertation. We would also like to thank CSIRO, Anglo American, Sumitomo Metal Mining, and The Aerospace Corporation for collecting the data.

## REFERENCES

- Abrams, M.J., Brown, D., Lepley, L., and Sadowski, R. (1983) Remote sensing of porphyry copper deposits in southern Arizona. *Economic Geology and the Bulletin of the Society of Economic Geologists*, v. 78, no. 4, p 591-604.
- Christensen, P.R., Bandfield, J.L., Hamilton, V.E., Howard, D.A., Lane, M.D., Piatek, J.L., Ruff, S.W., and Stefanov, W.L. (2000) A thermal emission spectral library of rock-forming minerals. *Journal of Geophysical Research*, v. 105, p. 9735-9739.
- Clark, R.N., Gallagher, A.J., and Swayze, G.A. (1990) Material absorption and band depth mapping of imaging spectrometer data using the complete band shape least-squares algorithm simultaneously fit to multiple spectral features from multiple materials: in *Proceedings of the Third Airborne Visible/Infrared Imaging Spectrometer (AVIRIS) Workshop*, JPL Publication 90-54, p.176-186.
- Cudahy, T.J., Okada, K., Yamato, Y., Maekawa, M., Hackwell, J.A., and Huntington, J.F. (2000) Mapping skarn and porphyry alteration mineralogy at Yerington, Nevada using airborne hyperspectral TIR SEBASS Data. *CSIRO Exploration and Mining Report 734R*. 74p.
- Dilles, J.H., and Einaudi, M.T. (1992) Wall-rock interaction and hydrothermal flow paths about the Ann-Mason porphyry copper deposit, Nevada – A 6 km vertical reconstruction: *Economic Geology*, v.87, p.1963-2001.
- Dilles, J.H., and Proffett, J.M. (2000) Metallogensis of the Yerington Batholith, Nevada. in Dilles, J.H., Barton, M.D., Johnson, D.A., Proffett, J.M, and Einaudi, M.T., eds.: *Contrasting Styles of Intrusion-Associated Hydrothermal Systems*, Society of Economic Geologists Guidebook Series Volume 32, p45-54.
- Dilles, J.H., Einaudi, M.T., Proffett, J.M., and Barton, M.D., (2000) Overview of the Yerington Porphyry Copper District: Magmatic to Nonmagmatic Sources of Hydrothermal Fluids: Their Flow Paths and Alteration Effects on Rocks and Cu-Mo-Fe-Au Ores. in Dilles, J.H., Barton, M.D., Johnson, D.A., Proffett, J.M, and Einaudi, M.T., eds.: *Contrasting Styles of Intrusion-Associated Hydrothermal Systems*, Society of Economic Geologists Guidebook Series Volume 32, p55-66.
- Hackwell, J.A., Warren, D.W., Bongiovi, R.P., Hansel, S.J., Hayhurst, T.L., Mabry, D.J., Sivjee, M.G., Skinner, J.W. (1996) LWIR/MWIR Imaging Hyperspectral Sensor for Airborne and Ground-Based Remote Sensing, *Imaging Spectrometry II*,

- Proceedings of the International Society for Optical Engineering, v.2819, p.102-107.
- ASTER Spectral Library (<http://speclib.jpl.nasa.gov>), last accessed May 15, 2007.
- Lowell, J.D., and Guilbert J.M., (1970) Lateral and vertical alteration-mineralization zoning in porphyry ore deposits: Economic Geology and the Bulletin of the Society of Economic Geologists, v. 65, no. 4, p 373-408.
- Proffett, J.M., and Dilles, J.H. (1984) Geologic map of the Yerington district, Nevada: Nevada Bureau of Mines Geologic Map 77, scale 1:24000.
- Salisbury, J.W., Walter, L.S., Vergo, N., D'Aria, D.M. (1991) Infrared (2.1 – 25  $\mu\text{m}$ ) Spectra of Minerals, Johns Hopkins University Press.
- Spatz, D.M., and Wilson, R.T. (1995) Remote sensing characteristics of porphyry copper systems, western America Cordillera, in Pierce, F.W., and Bolm, J.G., eds.: Arizona Geological Society Digest, v.20, p-94-108.
- Windeler, D.S., and Lyon, R.J.P. (1991) Discriminating Dolomitization of Marble in the Ludwig Skarn near Yerington, Nevada Using High Resolution Airborne Infrared Imagery, Photogrammetric Engineering and Remote Sensing, v.57, no. 9, p.1171-1177.
- Young, S.J., Johnson, B.R., and Hackwell, J.A. (2002) An In-Scene Method for Atmospheric Compensation of Thermal Hyperspectral Data, Journal of Geophysical Research, v. 107 (D24), p. 4774-4793.